

## Predictive modeling of the length of prepared CNT by CVD through ANN-MPSO and GEP

Morteza Khosravi<sup>1,\*</sup>, Malihe Zeraati<sup>2</sup>

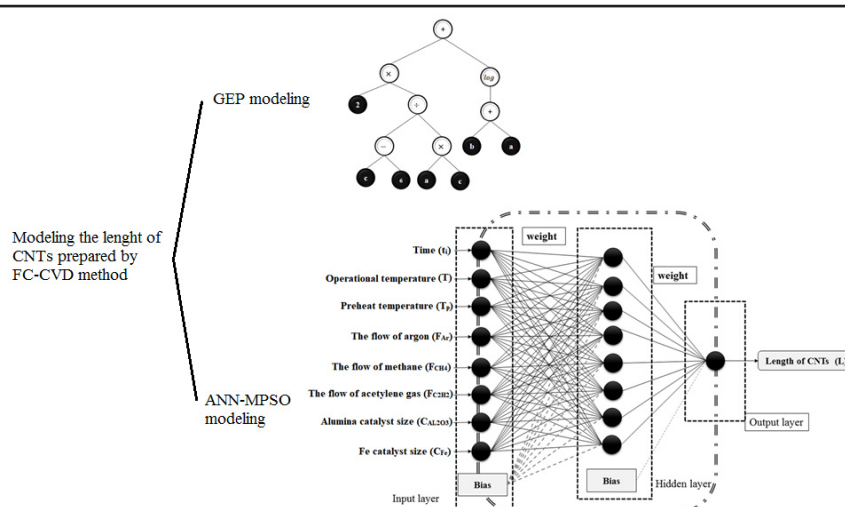
<sup>1</sup> Department of Materials Engineering, Faculty of Engineering, University of Sistan and Baluchestan, Zahedan, Iran

<sup>2</sup> Department of Materials Science and Engineering, Faculty of Engineering, Shahid Bahonar University of Kerman, Kerman, Iran

### HIGHLIGHTS

- This paper tried to model the length of CNTs prepared by FC-CVD.
- The modeling was performed by two methods: ANN-MPSO and GEP.
- It was confirmed through performance criteria analysis that the ANN-MPSO strategy performed better in the prediction of CNTs length than the GEP models.

### GRAPHICAL ABSTRACT



### ARTICLE INFO

#### Article history:

Received 03 October 2019

Revised 10 December 2019

Accepted 02 January 2020

#### Keywords:

Gene expression programming  
Hybrid artificial neural network  
Floating catalyst  
Carbon nanotubes length

### ABSTRACT

Floating catalyst chemical vapor deposition (FC-CVD) is considered as one of the most appropriate techniques for the preparation of carbon nanotubes (CNTs) on the industrial scale. This paper tried to model the length of CNTs prepared by FC-CVD using two approaches, i.e. gene expression programs and hybrid artificial neural networks. In this regard, the effect of various FC-CVD parameters, viz. temperature, time, preheat temperature, Ar gas flow, methane gas flow, ethylene gas flow, Al<sub>2</sub>O<sub>3</sub> catalyst, and Fe catalyst, on the length of CNTs, were investigated. At first, a hybrid artificial neural network-modified particle swarm optimization strategy (ANN-MPSO) has been used to model the CNTs length as a function of practical variables. In the next step, the same modeling of the problem was done using gene expression programming (GEP) instead of ANN-MPSO. The accuracy of the developed hybrid ANN-MPSO and GEP models was compared with regard to the linear combination of mean absolute percentage error and correlation coefficient as criteria. The results confirmed that the ANN model upgraded by the meta-heuristics strategy could be effectively applied for an accurate predictive model in the estimation of the length of CNTs as a function of the most important practical FC-CVD parameters. Also, the sensitivity analysis confirmed that the precursor type of carbon (including CH<sub>4</sub> and C<sub>2</sub>H<sub>4</sub>) and the preheat temperature have the highest and the least effect on the length of CNTs, respectively.

\* Corresponding author: Tel.: +9854-31132838 ; Fax: +9854-33447092 ; E-mail address: mkhosravi@eng.usb.ac.ir

DOI: 10.22104/JPST.2020.3835.1156

## 1. Introduction

Carbon nanotubes (CNTs), i.e., a one-dimensional allotrope of carbon, have been introduced as the strongest structure ever known [1]. The unique mechanical properties of CNTs make it an excellent candidate for the construction of advanced materials [2]. There are three main techniques for the preparation of CNTs, arc discharge [3-6], laser ablation [7,8], and chemical vapor deposition (CVD) [9-11]. All of these prepare CNTs of high-quality as well as high yield [14-17]. Compared to the laser ablation and arc discharge techniques, the CVD method is better at managing the practical parameters to prepare or tailored a CNT structure.

Based on the CVD method, various technologies have been developed for the preparation of CNTs for industry, including the floating catalyst, fluidized bed, and super-growth methods. The floating-catalyst CVD (FC-CVD) method injects the nanoparticles into a vertical furnace in the presence of a carbon precursor and prepare CNTs. Table 1 compares the various specification of CVD methods for mass production of CNTs. As can be seen, using the criteria of efficiency, purity, scalability, and quality, the FC-CVD method is strongly suggested for the preparation of CNTs with respect to the fluidized bed and super-growth methods.

Table 2 summarizes the various researches in the field of FC-CVD. Accordingly, there are several dependency relationships between the practical parameters of CNTs preparation, viz., operational temperature ( $T$ ), time of the process ( $t_i$ ), preheat temperature ( $T_p$ ), the flow of argon ( $F_{Ar}$ ), the flow of methane ( $F_{CH_4}$ ), the flow of ethylene ( $F_{C_2H_4}$ ), alumina catalyst size ( $C_{Al_2O_3}$  size), Fe catalyst size ( $C_{Fe}$  size) and the length of the desired prepared CNTs ( $L$ ). This length varies in the range of

0.03  $\mu\text{m}$  [13] to 201.6  $\mu\text{m}$  [14].

To the best of our knowledge, investigation and optimization of FC-CVD practical parameters has been carried out by various strategies, but a comprehensive study on the modeling of CNTs length by the FC-CVD technique has not yet been presented. The advantages of CVD include its ability to be scaled up for production at industrial levels as well as providing the control of process practical parameters over the morphology and the CNTs structure. Additionally, CVD's key role in CNTs preparation at the macroscopic size encourages us to investigate the predictive ability of the most common modeling approaches in artificial intelligence for the prediction of the length of CNTs prepared by FC-CVD.

In this study, a hybrid artificial neural network-modified particle swarm optimization (ANN-MPSO) and gene expression programming (GEP) strategies were separately employed for modeling of the length of prepared CNTs as a function of practical parameters of FC-CVD process. The most important point of these modeling strategies is their ability to generate science from the predicted data. The performance of the ANN is strongly dependent on its architecture, weights, and bias. Accordingly, automatic determination of ANN architecture, called the constrictive algorithm, is the main subject of many studies [22-25].

In this study, optimization of ANN parameters was carried out using MPSO, one of the most common heuristic algorithms. Acceptable flexibility, calculation cost, easy implementation, and consistent performance are the main advantages of particle swarm optimization (PSO). Unfortunately, during the implementation of PSO, in the case of the presence of local solutions in the search space, it is possible to trap the particles into the local optimum instead of absolute optimum. To counter this and other problems, in this paper we used a modified PSO (MPSO) to overcome the weaknesses of PSO like local optima and leverage of the ability of all underlying algorithms. A MPSO algorithm uses the crossover and mutation operators of a genetic algorithm to improve performance instability and global convergence [25].

A new predictive model utilizing gene expression programming (GEP) has been proposed, and then the accuracy of ANN-MPSO and GEP have been compared to each other. This study tries to show a reliable predictive model based on collected practical data by employing hybrid ANN-MPSO and GEP as a prediction strategy to determine the length of CNTs.

**Table 1.** Comparison of the most common CVD methods for mass production of CNTs [12].

	Floating catalyst	Fluidized bed*	Super-growth
Temperature	High	Medium	Medium
Efficiency	⊕	⊕	⊖
Purity	⊕	×	⊖
Scalability	⊕ (2D → 3D)	⊖ (3D)	Δ (2D)
Alignment	Δ	×	⊖
Quality	⊖	⊕	⊕

\* Rotary kiln with supported catalyst.

Quality: ⊖:Excellent ; ⊕:Good ; ×:Bad ; Δ:Unknown or depends

**Table 2.** Summary of the practical parameters for the preparation of CNTs using the FC-CVD method.

Reference	Year	Operational temperature (°C)	Time of process (min)	Preheat temperature (°C)	Flow of Ar (sccm)	Catalyst size (nm)		Flow of carbon precursor (sccm)		Length of CNTs (μm)
						Al <sub>2</sub> O <sub>3</sub>	Fe	CH <sub>4</sub>	C <sub>2</sub> H <sub>4</sub>	
Xiong <i>et al.</i> [15]	2006	730-840	500	25	400	10	1	-	75	0.4-12.42
Zhou <i>et al.</i> [16]	2006	700-875	20-45	750-900	25	10	3	-	100	0.2-7
Li <i>et al.</i> [17]	2006	755	30	770	25.51-1000	10	1.2	400	-	0.734-1.635
Einarsson <i>et al.</i> [18]	2008	690-840	65-390	25	400	10	1	-	75	0.2-12.42
Meshot <i>et al.</i> [19]	2009	725-825	15	980-1070	180	10	1	-	120	0.5-3.5
Choi <i>et al.</i> [20]	2010	780	3-16.7	780	1000	40	0.5-5	-	800	0.095-0.92
Wen <i>et al.</i> [14]	2010	1000	8.1-160	900	100	0	0	40	-	40.6-201.6
Nessim <i>et al.</i> [21]	2012	800	12	60	201-351	15	1	-	349.5-498.3	0.309-0.774
Li <i>et al.</i> [13]	2015	800	12	60	377-697	15	1	-	4.8-323.6	0.03-1.381

In summary, the main contributions of the current study are: Comprehensive modeling of the length of CNT prepared by chemical vapor deposition; Optimization of ANN weights and biases through modified PSO modeling; Application of ANN Modified PSO for sensitivity analysis of the length of CNT; Using GEP to predict the length of the prepared CNT; Comparison of the predictive ability of ANN Modified PSO and GEP.

## 2. Background

This section will provide a general background regarding the artificial neural network, particle swarm optimization, integration of genetic operators with particle swarm optimization, and gene expression programming.

### 2.1. Artificial Neural Network (ANN)

ANN is a powerful technique for optimization, solving problems, and prediction and is widely employed in many fields [26,27]. ANN consists of a lot of nonlinear element named neurons. The neurons in each layer are linked to the neurons in the other layers by a series of a math function. These functions employ a series of coefficient and constant values called weight and bias, respectively. If you consider  $f(x)$  as one of this functions, it is defined as below [28,29]:

$$f(x) = f\left(\sum_{i=1}^p w_i x + b\right) \quad (1)$$

Depending on the type of relations among each layer, this function can change. There are various transfer functions including the log-sigmoid (Logsig: Eq. (2)), tan-sigmoid (Tansig: Eq. (3)), and linear transfer function (Purlin: Eq. (4)). Operation of this function between neurons causes the production of a series of outputs. The accuracy of the ANN operation can be determined by comparing these values with the main values. Through simulation with ANN, the selection of network type, number of layers, number of neurons in each layer, and the type of transition function play a key role in network operation [30].

$$a(n) = \frac{1}{1 + \exp(-n)} \quad (2)$$

$$a(n) = \frac{-\exp(-2n)}{1 + \exp(-2n)} \quad (3)$$

$$a(n) = n \quad (4)$$

Today, the back propagation algorithm is the workhorse of learning in neural networks. Although this strategy has advantages, such as accuracy and versatility, it also suffers from disadvantages, e.g., being time-consuming and complex. The optimal values of the network weights/biases for the input-hidden (layer) and hidden-output (layer) in ANN architecture dictate its efficiency, but the manual determination of these values is a tedious process. These weights/biases can be optimized for the whole architecture to minimize the cost function and obtain a global optimum. Generally, the PSO algorithm is used to search the global space of

the developed ANN model to find the optimal weights/bias values. In this paper, we used a modified particle swarm optimization algorithm to compensate for the insufficiency of the back-propagation algorithm.

## 2.2. Particle swarm optimization algorithm (PSO)

PSO was initially proposed by Kennedy and Eberhart [24,31] and has been successfully applied in many applications [7,24,31]. The system is initialized randomly and the particles fly through the multi-dimensional search space at a certain velocity. Each particle represents a point in space and is associated with a velocity that indicates the direction of the particle. As the particles move throughout the space, each retains knowledge of its local best value (personal best). Since, the system is completely interconnected, a particle also retains knowledge of the overall best value (global best) of the objective function found thus far for the entire vicinity. Each individual emulates its most successful neighbor by updating its velocity and position to follow the most successful position of neighbors [32]. At the same time, the particle moves toward its own previous best position if it is the global best solution. Eventually, all particles will gather around the optimal value. The pseudocode of standard PSO is shown in Fig. 1.

However, the standard PSO is likely to become entrapped in the local optimal, which leads to a premature convergence phenomenon. To solve this problem, we used the modified PSO algorithm, which applies crossover and mutation operators to progress towards the global optimum, to search through the wider area [33,34].

1.	Begin
2.	$t=0$ ;
3.	Initialize particles $P(t)$ ;
4.	Evaluate particles $P(t)$ ;
5.	While (termination conditions are unsatisfied)
6.	Begin
7.	$t= t+1$ ;
8.	Update weights
9.	Select pBest for each particle
10.	Select gBest from $P(t-1)$ ;
11.	Calculate particle velocity $P(t)$ ;
12.	Update particle position $P(t)$ ;
13.	Evaluate particles $P(t)$ ;
14.	End
15.	End

Fig. 1. Pseudocode of PSO.

## 2.3. Modified particle swarm optimization (MPSO)

If particles find the best position is a local optimum when they are moving through the solution space, they cannot explore the problem space again. Du *et al.* [33] developed a hybrid PSO strategy that incorporates operators from GA into PSO. They compared the performance of the proposed method with GA and standard PSO in artificial neural networks weight training, and proved its superiority. In addition, Shi *et al.* [34] claimed that a combination of PSO with GA operators can alleviate some limitations of PSO.

Consequently, the back-propagation based classical ANN training methods can be integrated with MPSO to refine an initially random set of weights to achieve a better estimate close to the global optimum of the architecture space. Using this logic, we attempted to increase the accuracy of CNTs length prediction prepared by FC-CVD based on the ANN-MPSO technique. Figs. 2(a) and 2(b) illustrate the general structure and (b) detailed computational flowchart of the ANN-MPSO implemented in this study.

## 2.4. Gene expression programming (GEP)

Gene expression programming (GEP) introduced by Ferreira [36] is the enhanced version of gene programming (GP) [35]. Accordingly, GEP contains the main advantage of GP, i.e., the selection of the most appropriate solution by checking all of the possibilities using computer software [37]. The main components of GEP are the termination condition, control parameters, fitness function, terminal set, and function set [38].

Expression tree (ET) is the most common methodology for the illustration of the solution population generated by GEP. The typical ET for Eq. (5) is illustrated in Fig. 3.

$$2 \times ((c-6)/(a \times c)) + \log(a-b) \quad (5)$$

At the beginning of GEP analysis, the user must be set the number of terminals and primitive functions for every branch of the to-be-evolved program, select the fitness criteria, determine the parameters of run controlling, and select the termination rule of the designation strategy for the illustration results [39]. In summary, the GEP steps can be summarized as follows [36,40].

- (1) Creation of initial population with a random

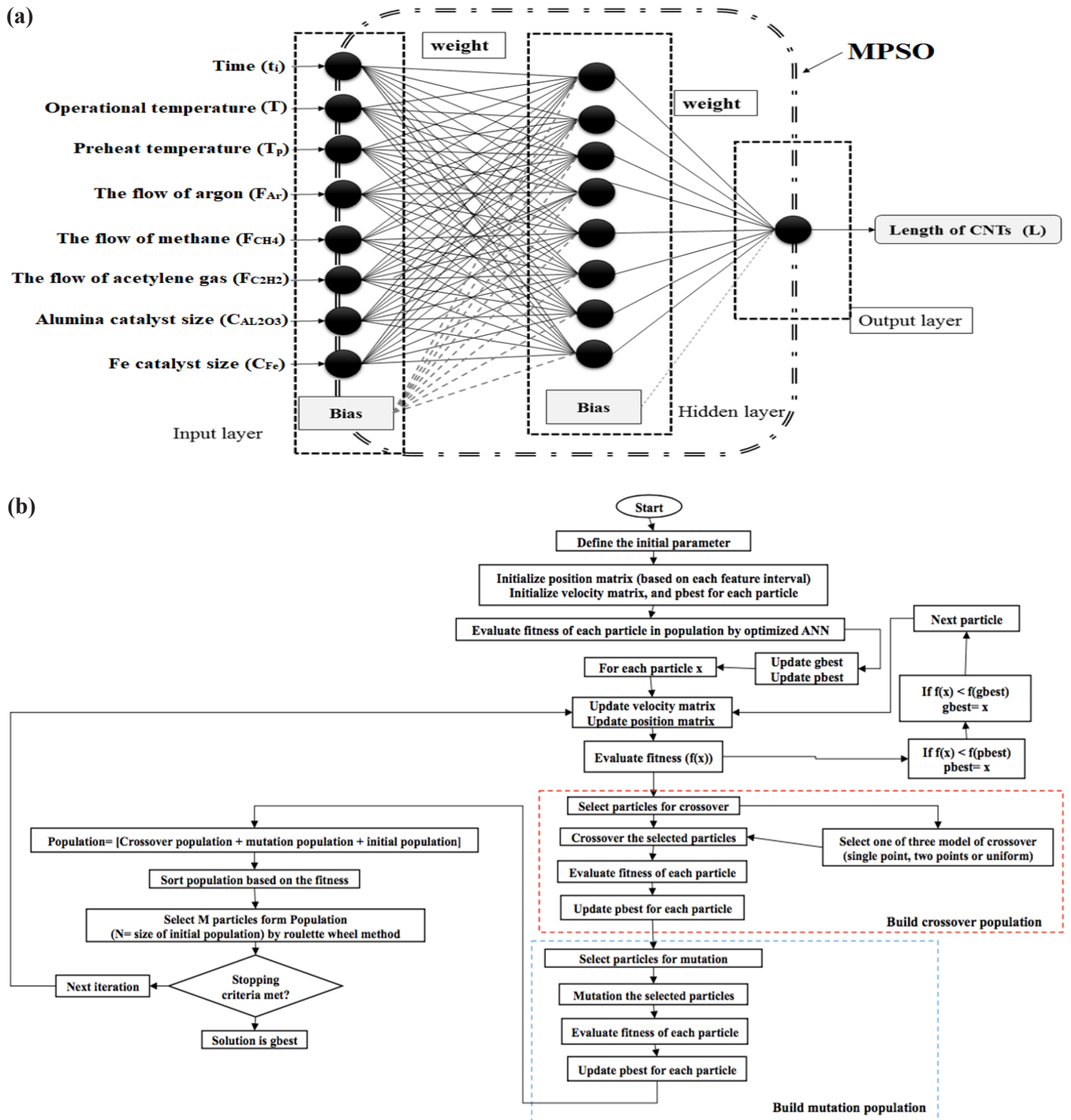


**Fig. 2.** (a) Architecture and (b) computational flowchart of ANN-MPSO implementation structure and in the prediction of CNTs length as a function of FC-CVD practical parameters.

distribution of terminals and functions of the issues using computer software;

(2) Execute each state in the proposed population and determine the relevant fitness value as a criterion for its problem-solving ability;

(3) Employ program software mutation and crossover to select the best existing programs for new population generation;

(4) After Comparing the best program after any

generation with the best solution of all generations, the best generation is saved as the genetic result of the modeling. This study tried to use the GEP as a new approach for proposing empirical models to determine the CNTs length by chemical vapor deposition.

Characteristics of GEP, including function set, head size, and chromosome type, were adjusted based on the iterators [47,48,50]. Fig. 4 shows several steps of gene expression programming modeling.

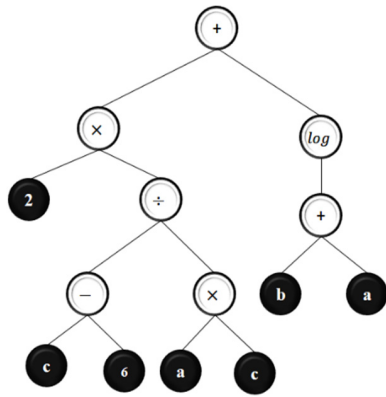


Fig. 3. Typical representation of expression tree for Eq. (5).

3. Experimental data collection

Generally, the determination of the effective practical process is considered the main step for optimization strategies. By considering the reported works about the preparation of CNTs by FC-CVD, there are eight effective parameters including the operational temperature, time of the process, preheat temperature, flow rate of argon, flow rate of carbon source, size, and type of catalyst particles.

The main goal of this study is to upgrade experimental results to the industrial scale, using methane and ethylene as carbon sources. Fe and alumina nanoparticles were selected as candidates for the metallic and ceramic type of catalyst, respectively. Table 3 abbreviates the FC-CVD practical parameters for the preparation of CNTs in the current study. In Table 3,  $T$ : temperature,  $t_i$ : time,  $T_p$ : preheat temperature,  $F_{Ar}$ : the flow of argon,  $F_{CH_4}$ : the flow of methane gas,  $F_{C_2H_4}$ : the flow of ethylene gas,  $C_{Al_2O_3}$  size: alumina catalyst size,  $C_{Fe}$ : Fe catalyst size, and  $L$ : the length of prepared CNTs.

Table 3. Explanation of CVD parameters and their dimensions in this work [13-17,19,20].

No.	$T$	$t_i$	$F_{Ar}$	$T_p$	$F_{C_2H_4}$	$F_{CH_4}$	$C_{Al_2O_3}$	$C_{Fe}$	$L$
1	825	15	180	1020	0	120	10	1	3.5
2	825	15	180	1000	0	120	10	1	3.3
3	825	15	180	980	0	120	10	1	2.65
4	825	15	180	1040	0	120	10	1	1.2
5	825	15	180	1070	0	120	10	1	0.9
6	875	15	180	1020	0	120	10	1	2.1
7	775	15	180	1020	0	120	10	1	1.1
8	725	15	180	1020	0	120	10	1	0.5
9	780	390	400	25	0	75	10	1	12.42
10	780	325	400	25	0	75	10	1	10.83
11	780	265	400	25	0	75	10	1	9.02
12	780	130	400	25	0	75	10	1	4.75
13	780	65	400	25	0	75	10	1	2.53
14	730	390	400	25	0	75	10	1	5.50
15	750	390	400	25	0	75	10	1	8.65
16	800	390	400	25	0	75	10	1	8.05
17	820	390	400	25	0	75	10	1	2.00
18	840	390	400	25	0	75	10	1	0.40
19	690	390	400	25	0	75	10	1	0.20
20	730	500	400	25	0	75	10	1	5.50
21	750	500	400	25	0	75	10	1	8.65
22	780	500	400	25	0	75	10	1	12.42
23	800	500	400	25	0	75	10	1	8.05
24	820	500	400	25	0	75	10	1	2.00
25	840	500	400	25	0	75	10	1	0.40
26	1000	32.4	100	900	40	0	0	0	40.60
27	1000	83.4	100	900	40	0	0	0	100.75
28	1000	121.7	100	900	40	0	0	0	151.20
29	1000	160	100	900	40	0	0	0	200.00
30	1000	32.4	100	900	40	0	0	0	40.60
31	1000	83.4	100	900	40	0	0	0	100.75
32	1000	121.7	100	900	40	0	0	0	151.20
33	1000	160	100	900	40	0	0	0	200
34	1000	16.2	100	900	40	0	0	0	41
35	1000	62.6	100	900	40	0	0	0	150.70
36	1000	81.1	100	900	40	0	0	0	201.60
37	1000	16.2	100	900	40	0	0	0	41
38	1000	40.5	100	900	40	0	0	0	98.30
39	1000	62.6	100	900	40	0	0	0	150.70

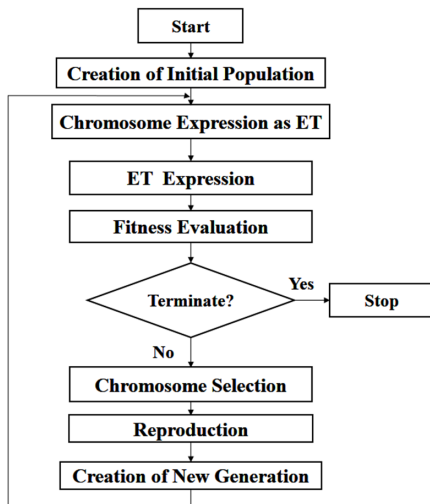


Fig. 4. Schematic representation of GEP strategy [33].

**Table 3.** *to be continued*

No.	$T$	$t_i$	$F_{Ar}$	$T_p$	$F_{C_2H_4}$	$F_{CH_4}$	$C_{Al_2O_3}$	$C_{Fe}$	$L$
40	1000	81.1	100	900	40	0	0	0	201.60
41	1000	8.1	100	900	40	0	0	0	41.00
42	1000	18.5	100	900	40	0	0	0	98.70
43	1000	30.1	100	900	40	0	0	0	151.4
44	1000	40.5	100	900	40	0	0	0	199.1
45	760	45	25	875	0	100	10	3	7
46	760	30	25	760	0	100	10	3	1
47	760	30	25	760	0	100	10	3	0.7
48	760	45	25	875	0	100	10	3	0.7
49	760	20	25	750	0	100	10	3	0.45
50	760	20	25	800	0	100	10	3	3.1
51	760	20	25	850	0	100	10	3	4.5
52	760	20	25	900	0	100	10	3	5
53	760	20	25	950	0	100	10	3	0.45
54	765	20	25	875	0	100	10	3	4.8
55	800	20	25	875	0	100	10	3	2.5
56	812	20	25	875	0	100	10	3	0.3
57	875	20	25	875	0	100	10	3	0.2
58	725	20	25	875	0	100	10	3	2.2
59	700	20	25	875	0	100	10	3	0.4
60	755	30	25.51	770	400	0	10	1.2	1.347
61	755	30	53.57	770	400	0	10	1.2	1.567
62	755	30	100	770	400	0	10	1.2	1.635
63	755	30	250	770	400	0	10	1.2	1.539
64	755	30	500	770	400	0	10	1.2	1.635
65	755	30	750	770	400	0	10	1.2	1.01
66	755	30	1000	770	400	0	10	1.2	0.734
67	800	12	696.75	60	0	4.80	15	1	0.03
68	800	12	677.273	60	0	24.27	15	1	0.192
69	800	12	651.299	60	0	50.16	15	1	0.476
70	800	12	626.98	60	0	74.43	15	1	0.718
71	800	12	600.974	60	0	100.32	15	1	0.984
72	800	12	576.623	60	0	124.59	15	1	1.13
73	800	12	550.64	60	0	150.49	15	1	1.288
74	800	12	501.94	60	0	199.03	15	1	1.381
75	800	12	453.24	60	0	247.58	15	1	1.152
76	800	12	425.649	60	0	275.08	15	1	1.022
77	800	12	399.675	60	0	300.97	15	1	0.91
78	800	12	376.94	60	0	323.63	15	1	0.8486
79	800	12	350.97	60	0	349.52	15	1	0.774

**Table 3.** *to be continued*

No.	$T$	$t_i$	$F_{Ar}$	$T_p$	$F_{C_2H_4}$	$F_{CH_4}$	$C_{Al_2O_3}$	$C_{Fe}$	$L$
80	800	12	325	60	0	375.41	15	1	0.693
81	800	12	300.64	60	0	399.67	15	1	0.619
82	800	12	276.29	60	0	423.94	15	1	0.538
83	800	12	251.94	60	0	448.22	15	1	0.458
84	800	12	225.974	60	0	474.11	15	1	0.384
85	800	12	201.623	60	0	498.38	15	1	0.309
86	780	16.7	1000	780	0	800	40	0.5	0.92
87	780	8.3	1000	780	0	800	40	1	0.55
88	780	8.7	1000	780	0	800	40	2	0.61
89	780	3.0	1000	780	0	800	40	5	0.095

**4. Pre-processing of collected data**

Before continuing with the modeling, a simple pre-processing of the data to find the best performance has been carried out. In this regard, a boxplot was used as a simple and common method to show the distribution of the practical data set and outlier, graphically [41]. Fig. 5 showed the boxplot of the input data set considering eight practical parameters. As can be seen, there is no outlier in any of the parameters and the medium of each parameter for all datasets (exception of  $t_i$ ) shows a symmetric distribution.

Further pre-processing of data was carried out by checking the independence of the practical data, as a critical approach to modeling. To achieve this goal, a bivariate correlation analysis was utilized. This analysis enables us to determine the amount and direction of the interaction of practical parameters with each other.

Accordingly, we found that a high positive or negative

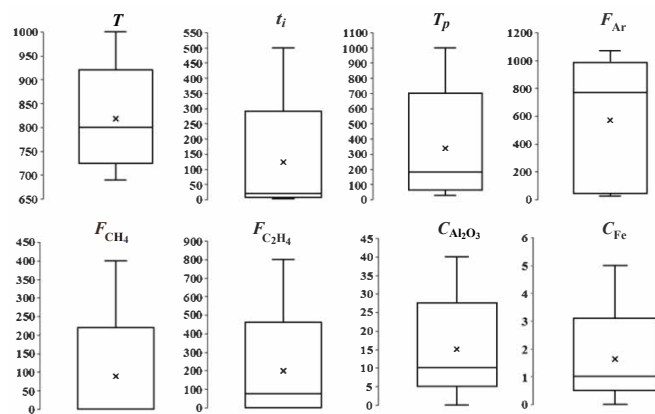


**Fig. 5.** Boxplot of FC-CVD practical dataset for the preparation of CNTs.

correlation coefficients among the pairs decreased the performance of the proposed ANN-MPSO model, significantly [14,21]. Table 4 summarized the bivariate correlation matrix of FC-CVD practical parameters according to the Pearson's correlation coefficients among the practical parameters. As can be seen in Table 4, there is little interaction between FC-CVD practical parameters, except in the case of  $(T, C_{Al_2O_3})$ ,  $(T, C_{Fe})$  and  $(T_p, C_{Al_2O_3})$  pairs.

Principal component analysis (PCA) is a powerful approach for dimension reduction in the case of the presence of interaction between the input data. PCA provides the possibility of transformation from multidimensional space to lower dimension space. In this case, the correlation between the variable in the new space must be removed [42-44]. Kaiser Mayer Olkin (KMO) proposed Eq. (6) as criteria for the necessity of PCA in the case of the presence of interaction between the input dataset [45].

$$KMO = \frac{\sum \sum r_{ij}^2}{\sum \sum r_{ij}^2 + \sum \sum a_{ij}^2} \quad (6)$$

In which,  $r_{ij}$  and  $a_{ij}$  are the correlation coefficient and a practical correlation coefficient of  $i$  and  $j$  variables, respectively. In the case of  $KMO < 0.7$ , the dependency between practical parameters is unreal and must be neglected [46]. The KMO factor for FC-CVD practical parameters is estimated at 0.476, i.e., lower than 0.7, and as a consequence, the data used in the current study are suitable for further modeling.

## 5. Results and discussion

Statistical indices, including the correlation coefficient ( $R^2$ ; Eq. (7)), mean absolute percentage error (MAPE;

Eq. (8)) and root means square error (RMSE; Eq. (9)), were used to investigate the performance and accuracy of the optimal proposed ANN-MPSO network and GEP model. The equations for the estimation of the above indicators are:

$$R^2 = 1 - \frac{\sum_{i=1}^n (y_a - y_p)^2}{\sum_{i=1}^n (y_a - \bar{y}_a)^2} \quad (7)$$

$$MAPE = \frac{1}{N} \sum_1^N \left( \frac{|y_a - y_p|}{y_a} \times 100 \right) \quad (8)$$

$$RMSE = \sqrt{\frac{1}{N} \sum_1^N (y_p - y_a)^2} \quad (9)$$

In which,  $y_a$  is the actual value,  $y_p$  is the predicted value, and  $N$  is the total number of datasets, i.e.,  $N=89$  in the current study. The input space of the ANN model is optimized using the MPSO algorithm, with the objective of maximization of  $R^2$  (closer to 1) and simultaneously minimization of RMSE and MAPE (closer to 0). Table 5 summarizes a list of the 10 most appropriate networks with statistical indices as criteria.

As shown in Table 5, ANN-MPSO 8, with the highest value of  $R^2$  (i.e., 0.8446) as well as the lowest value of MAPE (i.e., 2.6334), was selected as most appropriate model network for the prediction of CNTs length. While, in the case of lower RMSE as criteria for selection of most appropriate network, ANN-MPSO 2 with a RMSE equal to 0.0006 was proposed the optimal network.

After checking over than 100 GEP models, Table 6 shows various GEP model combinations generated by different GEP parameters, such as chromosome number, head size, gen number, linking function, and function set, were investigated to find the best GEP model to

**Table 4.** Correlation coefficients of  $T$ ,  $t_i$ ,  $T_p$ ,  $F_{Ar}$ ,  $F_{CH_4}$ ,  $F_{C_2H_4}$ ,  $F_{C_2H_4}$ ,  $C_{Al_2O_3}$  and  $C_{Fe}$ .

Parameters	$T$	$t_i$	$T_p$	$F_{Ar}$	$F_{CH_4}$	$F_{C_2H_4}$	$C_{Al_2O_3}$	$C_{Fe}$
$T$	1.000	-0.129	-0.337	0.392	-0.091	-0.310	-0.603	-0.636
$t_i$	-0.129	1.000	0.133	-0.498	-0.150	-0.211	-0.115	-0.153
$T_p$	-0.337	0.133	1.000	-0.474	0.050	0.519	0.725	-0.042
$F_{Ar}$	0.392	-0.498	-0.474	1.000	0.233	-0.189	-0.282	0.103
$F_{CH_4}$	-0.091	-0.150	0.050	0.233	1.000	-0.268	-0.111	-0.090
$F_{C_2H_4}$	-0.310	-0.211	0.519	-0.189	-0.268	1.000	0.864	0.258
$F_{C_2H_4}$	-0.603	-0.115	0.725	-0.282	-0.111	0.864	1.000	0.429
$C_{Fe}$	-0.636	-0.153	-0.042	0.103	-0.090	0.258	0.429	1.000

**Table 5.** Representation of  $R^2$ , MAPE, and RMSE for the 10 most appropriate ANN-MPSO structures.

Model	Neurons	Function	$R^2$	MAPE	RMSE
ANN-MPSO 1	8-7-1	logsig-purelin	0.8170	3.9337	0.0153
ANN-MPSO 2	8-4-1	tansig-purelin	0.7992	4.2223	0.0006
ANN-MPSO 3	8-8-1	tansig-purelin	0.8181	3.9142	0.0021
ANN-MPSO 4	8-3-1	logsig-purelin	0.7837	4.2699	0.0041
ANN-MPSO 5	8-14-1	logsig-purelin	0.7937	3.6650	0.0019
ANN-MPSO 6	8-12-1	tansig-purelin	0.8307	3.2747	0.0020
ANN-MPSO 7	8-17-1	logsig-purelin	0.8058	3.9243	0.0062
ANN-MPSO 8	8-28-1	logsig-purelin	0.8446	2.6334	0.0045
ANN-MPSO 9	8-25-1	tansig-purelin	0.7809	5.5519	0.0103
ANN-MPSO 10	8-16-1	logsig-purelin	0.7730	4.8343	0.0209

**Table 6.** GEP models with applied parameters.

Model	Linking function	Head size	Number of genes	Type of function	$R^2$	MAPE	RMSE
GEP-1	Multiplication	9	3	F4	0.9449	13.7344	0.2345
GEP-2	Addition	9	4	F1	0.9902	5.7873	0.0988
GEP-3	Addition	9	3	F2	0.9657	10.8462	0.1852
GEP-4	Multiplication	9	4	F3	0.9849	7.1910	0.1228
GEP-5	Multiplication	8	4	F3	0.9855	7.2044	0.1230
GEP-6	Addition	9	4	F3	0.9722	10.2235	0.1746
GEP-7	Addition	8	4	F4	0.9750	9.2902	0.1586
GEP-8	Addition	9	3	F4	0.9188	17.4956	0.2988
GEP-9	Multiplication	8	3	F1	0.9911	5.7536	0.0982
GEP-10	Multiplication	9	4	F1	<b>0.9943</b>	<b>4.4040</b>	<b>0.0752</b>

explain CNTs length values. Table 7 illustrates several function sets that have been employed through the construction of GEP models.

Similar to the ANN-MPSO modeling approach, the accuracy and the performance of the proposed GEP models have been investigated with statistical indices, i.e.,  $R^2$ , MAPE, and RMSE. The parametric and statistical details of the selected GEP model are shown in Table 8. Comparison of GEP-9 and GEP-10 revealed that higher chromosome, as well as gene numbers,

increased the accuracy of the constructed GEP models. Similar results have been observed through the use of addition and multiplication as linking functions. Using higher  $R^2$  values (closer to 1) and lower errors indices or MAPE, and RMSE values closer to 0 as criteria for selection of the best GEP model revealed that GEP 10 with  $R^2 = 0.9943$ , MAPE = 4.4040 and RMSE = 0.0752 satisfied all thresholds. The expression tree for the four sub-genes of GEP 10 is given in Fig. 6.

As shown in Fig. 6, there is a complicated dependency between the selected practical parameters and the length of prepared CNTs. The formulation of the length of CNTs ( $L$ ) values by the GEP model can be determined by a combination of Eqs. (10)-(14) for the prediction of CNTs length as a function of the experimental parameters of FC-CVD.

**Table 7.** Function sets used in the GEP models

Function set	Functions
F1	$+, -, \times, \sqrt{\quad}, /, \ln, \cos, x^2$
F2	$+, -, \times, /$
F3	$exp, log, x^2, -, \times, \cos, \sin$
F4	$log, x^2, \times, \sqrt{\quad}, \tan, \arcsin, 1/x, exp$

$$S_j = 7.8096 + \cos(0.1038 + T + 2t_i + 3.751C_j) \quad (10)$$

**Table 8.** Parametric and statistical details of the selected GEP model.

Parameter	Value
Chromosomes	42
Head size	9
Genes	4
Linking function	Multiplication
Function set	F1
Mutation rate	0.0026
Inversion rate	0.01
Constants per gene	10
Training sample	67
Testing sample	22
Fitness function	RMSE
$R^2$ training	0.9943
RMSE training	0.0752
MAPE training	4.4040
$R^2$ testing	0.9824
RMSE testing	0.0491
MAPE testing	2.0571

$$S_2 = -3.8194 + \cos(3.0152 - 2t_i + (t_i + F_{Ar}) \times (F_{Ar} - C_f)) \quad (11)$$

$$S_3 = -6.879 + \frac{t_i^2}{1. - 5.2892t_i + F_w \times C_a} \quad (12)$$

$$S_4 = \frac{2029.3164 \times C_f^2}{(-18.1659 + F_a)^2} \quad (13)$$

$$L = S_1 \times S_2 \times S_3 \times S_4 \quad (14)$$

Fig. 7 compares the CNTs length predicted by GEP 10 and experimental data.

To provide for a comparison of the predicting ability of ANN-MPSO and GEP modeling approaches, all statistical indices must be considered simultaneously. In this regard, utilization of a combined function, such as Eq. (15), can be useful to determine the best modeling

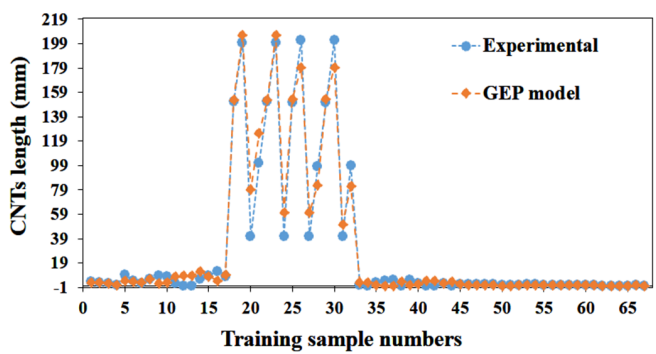


**Fig. 7.** Experimental and GEP model results for the length of CNTs.

approach for modeling CNTs length as a function of the practical parameters of FC-CVD. As defined, the lower value of the combined function can be considered as the criteria for the selection of the most appropriate model for the prediction CNTs length by the proposed ANN-MPSO and GEP approaches.

$$\text{Combined function} = 1/(R^2 + \text{MAPE} + \text{RMSE}) \quad (15)$$

Fig. 8 shows the combined function of the 10 most appropriate networks by ANN-MPSO as well as the 10 most appropriate GEP models. As shown, the minimum value of the combined function related to ANN-MPSO 7, ANN-MPSO 2, and ANN-MPSO 5 is 2.1667, 2.1737 and 2.3198, respectively. Accordingly, the ANN-MPSO 7 network with architecture 8-17-1 and activation function logsig-purlin is introduced as the most appropriate model for predicting the length of CNTs prepared by FC-CVD. Also, the higher neuron number of the first hidden layer (e.g., ANN-MPSO 2, ANN-MPSO 5, and ANN-MPSO 7) does not significantly change the combined function values. At a constant activation function of purlin in the second hidden layer, the activation function of logsig through the first hidden layer performed better with respect to the tansig. The predicting ability of ANN-MPSO

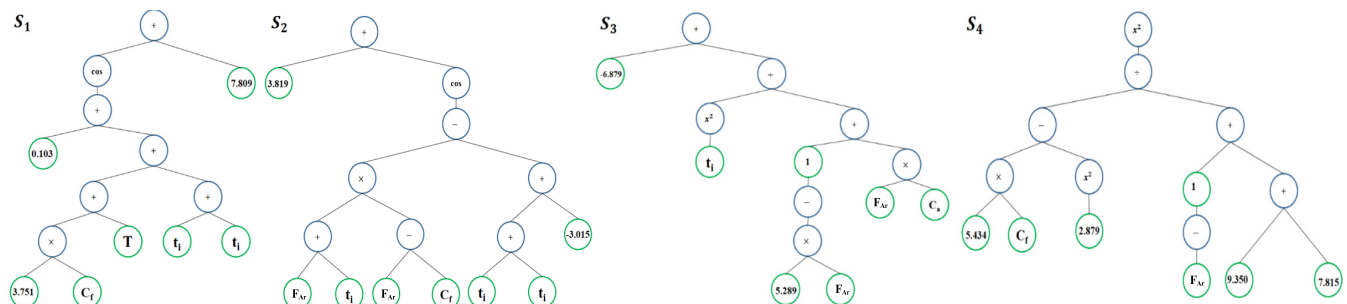


**Fig. 6.** Representation of the GEP-10 model as an expression tree.

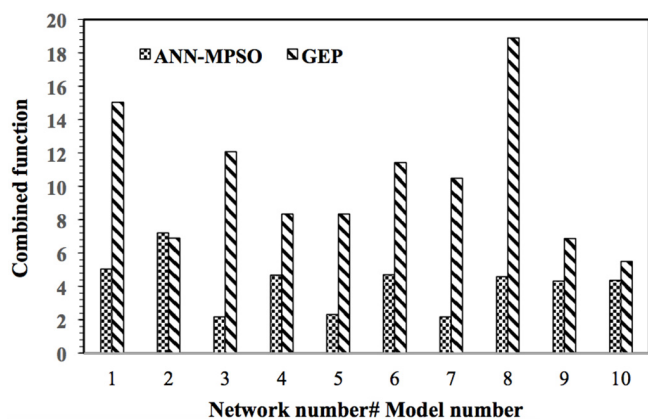


**Fig. 8.** Comparison of the 10 most appropriate ANN-MPSO networks and GEP models using a combined function as criteria.

in all cases is better than the GEP models. This may be due to the ability of MPSO to search all regions of each practical parameters and determine the absolute optimum instead of the local optimum.

The normalized predicted values for the input parameters are shown compared with the experimental data using ANN-MPSO 7 in Fig. 9. As can be seen, there is an acceptable agreement between the predicted and actual value of CNTs length, which confirms the predicting ability of the proposed method.

After determining the most appropriate model to predict the CNTs length, i.e., ANN-MPSO, sensitivity analysis was employed to determine the influence of eight effective practical variables in the developed ANN-MPSO network. Fig. 10 showed the results of the sensitivity analysis. Quantitative and qualitative analysis of the effect of each parameter is the main advantage of this analysis.

As shown in Fig. 10, the flow of  $\text{CH}_4$  and  $\text{C}_2\text{H}_4$ , i.e., the precursor of carbon, were the parameters that had the most effect on the length of CNTs. Both investigated carbon precursor in this study have linear structures, which encourage the formation of straight hollow CNTs as a consequence of thermal decomposition of  $\text{CH}_4$  and  $\text{C}_2\text{H}_4$  to linear trimers/dimers or atomic carbon [47,48]. Hence, the greater dependency of CNTs length on  $\text{CH}_4$  can be related to the higher hydrogen content with respect to  $\text{C}_2\text{H}_4$ . In this case, the higher hydrogen content of  $\text{CH}_4$  plays as etching role on the amorphous carbon as well as an being an effective reducing agent for oxide removal from the surface of the catalyst. These observations were contrast exactly to the carbon-rich precursors, which have shown higher CNTs yields. It seems that the reducing ability of hydrogen in  $\text{CH}_4$  can

be compensated for by the lower content of carbon in  $\text{CH}_4$ , with respect to  $\text{C}_2\text{H}_4$ . This behavior was intensified at higher operating temperatures (test number 26 to 44 in Table 3) and evolved as higher noise in the sensitivity analysis (Fig. 10). High curvature and small diameters of single-wall CNTs induced higher strain energy with respect to multi-wall CNTs, facilitating the growth of multi-wall CNTs, especially at low temperatures. Accordingly, the higher noises from the average value of each parameter in the cases of higher temperature can be related to the higher forms of multi-wall CNTs in FC-CVD at low temperatures (600-900 °C) with respect to the single wall CNTs, i.e., the administrated phase at higher operational temperatures 900-1200 °C [48].

After the carbon precursor, the time of the process, type of catalyst and operational temperature are situated at the next level that affects the length of CNTs. According to the literature [49], researchers are conflicted about the mechanisms of CNTs growth through FC-CVD. However, the most accepted mechanism of CNTs growth supposes that the precursor of carbon in gas phases are first adsorbed on the surface of the catalyst and then catalytically dissociated to its components in a way that carbon species diffused through the catalyst particles, and after supersaturation, seamless carbon cylinder (CNTs) are formed from its surface. In this mechanism, the prolonged time and temperature of the process enhance the possibility of higher diffusion, and as a consequence, longer CNT will be produced. The greater dependency of CNTs length to the Fe catalyst with respect to  $\text{Al}_2\text{O}_3$  can be related to the higher solubility and diffusion rate of carbon in the Fe alloy at operational temperatures of FC-CVD. Moreover, regarding  $\text{Al}_2\text{O}_3$ , the adhesion between Fe and CNTs growth are stronger. Consequently, the Fe catalyst is

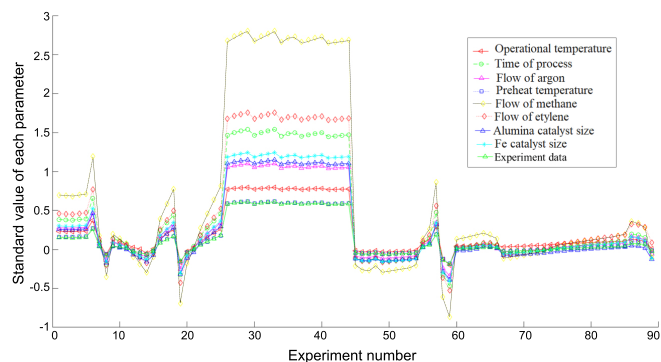


**Fig. 10.** Sensitivity analysis of the effect of practical parameters of FC-CVD on the length of prepared CNTs.

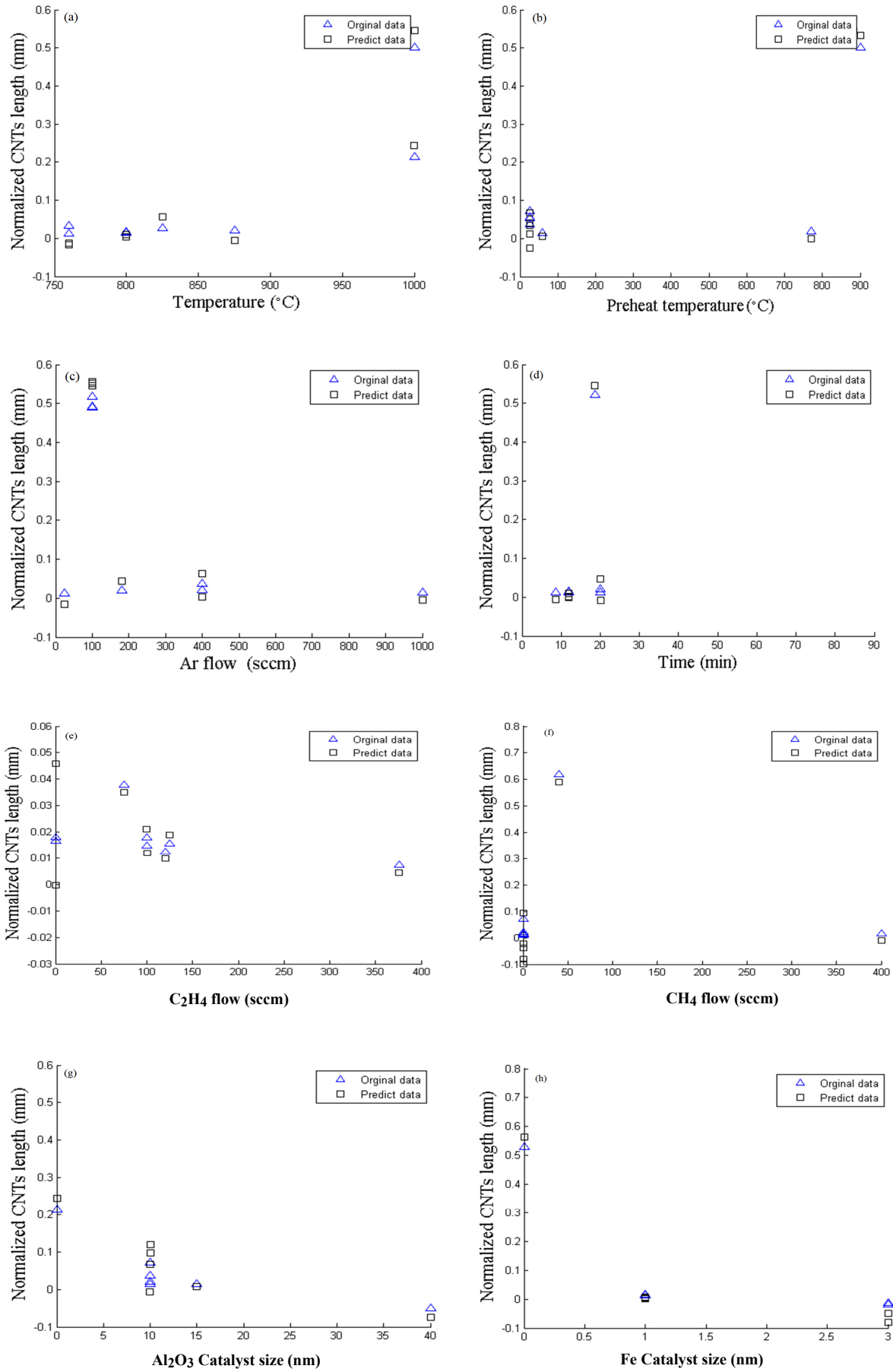


**Fig. 9.** Comparison of experimental data and ANN-MPSO structures for normalized CNTs length versus (a) Temperature (°C), (b) Preheat temperature (°C), (c) Flow of Ar (sccm), (d) Time (min), (e) C<sub>2</sub>H<sub>4</sub> Flow (sccm), (f) CH<sub>4</sub> Flow (sccm), (g) Al<sub>2</sub>O<sub>3</sub> Catalyst size (nm), and (h) Fe Catalyst size (nm).

more effective in the formation of longer CNTs with a lower diameter [50]. It seems that preheat temperature has no significant effect on the length of CNTs.

We investigated the behavior of proposed ANN-MPSO networks at various iterations using the fitness value (Eq. (16)) as criteria.

$$\text{Fitness value} = \frac{1}{N} \sum_{1}^N (y_a - y_p)^2 \quad (16)$$

Fig. 11 illustrates the dependency of the fitness value of the 10 most appropriate ANN-MPSO networks up to 100 iterations. As can be seen, all proposed networks showed a fitness value lower than 0.04 after about 10 iterations, revealing the acceptable performance of the proposed strategy with significantly lower estimation cost.

## 6. Conclusion

The predicting ability of the modified particle swarm optimization-artificial network approach was compared with gene expression programming to predict the length of carbon nanotubes prepared by chemical vapor deposition. To provide the dataset for modeling, 89 tests were employed by considering the main practical parameters of chemical vapor deposition, i.e., under various levels of temperature, time, preheat temperature, Ar gas flow, methane gas flow, ethylene gas flow, alumina catalyst, and Fe catalyst, as input variables for construction of predictive models. First, outlier data were removed and then the ANN-MPSO and GEP modeling parameters were tuned separately to find the models with the minimum combined function, i.e., a linear combination of  $R^2$ , MAPE, and RMSE, to predict the length of CNTs prepared by FC-CVD. Both models, ANN-MPSO and GEP, were compared with

the combined function as criteria. It was confirmed through performance criteria analysis that the ANN-MPSO strategy performed better in the prediction of CNTs length as compared to the GEP models. Also, sensitivity analysis confirmed that in the investigated range, the carbon precursor, process time, and type of catalysts were the parameters that had the most control on the length of the prepared CNT. Accordingly, the ANN-MPSO model upgraded with meta-heuristics is a promising tool to model industrial issues and can be employed to recognize practical interactions in the case of a well-trained structure.

## References

- [1] R. Zhang, Q. Wen, W. Qian, D.S. Su, Q. Zhang, F. Wei, Superstrong ultralong carbon nanotubes for mechanical energy storage, *Adv. Mater.* 23 (2011) 3387-3391.
- [2] B.C. Edwards, Design and deployment of a space elevator, *Acta Astronaut.* 47 (2000) 735-744.
- [3] N. Sano, H. Wang, M. Chhowalla, I. Alexandrou, G.A. Amaratunga, Nanotechnology: Synthesis of carbon 'onions' in water, *Nature*, 414 (2001) 506-507.
- [4] H. Zhu, X.S. Li, B. Jiang, C.L. Xu, Y.F. Zhu, D.H. Wua, X.H. Chen, Formation of carbon nanotubes in water by the electric-arc technique, *Chem. Phys. Lett.* 366 (2002) 664-669.
- [5] H. Lange, M. Sioda, A. Huczko, Y.Q. Zhu, H.W. Kroto, D.R.M. Walton, Nanocarbon production by arc discharge in water, *Carbon*, 41 (2003) 1617-1623.
- [6] M.V. Antisari, R. Marazzi, R. Krsmanovic, Synthesis of multiwall carbon nanotubes by electric arc discharge in liquid environments, *Carbon*, 41 (2003) 2393-2401.
- [7] A. Thess, R. Lee, P. Nikolaev, H. Dai, P. Petit, J. Robert *et al.*, Crystalline ropes of metallic carbon nanotubes, *Science*, 273 (1996) 483-487.
- [8] W. Liu, S.-P. Chai, A.R. Mohamed, U. Hashim, Synthesis and characterization of graphene and carbon nanotubes: A review on the past and recent developments, *J. Ind. Eng. Chem.* 20 (2014) 1171-1185.
- [9] R. Saito, G. Dresselhaus, M.S. Dresselhaus, *Physical Properties of Carbon Nanotubes*, Imperial College Press, London, 1998.

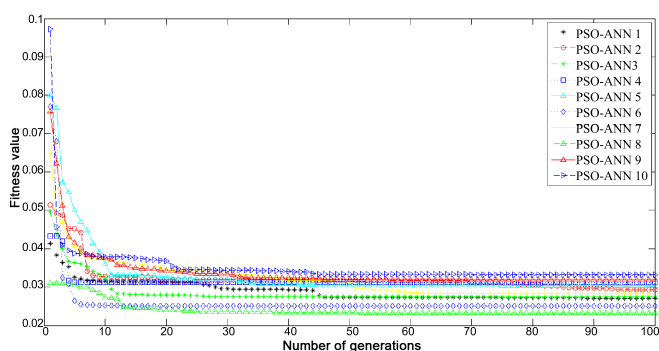


**Fig. 11.** Fitness values versus iteration number for different PSO-ANN structures.

- [10] P. Harris, Carbon Nanotubes and Related Structures, Cambridge University Press, Cambridge, 1999.
- [11] S. Iijima, Helical microtubules of graphitic carbon, *Nature*, 354 (1991) 56-58.
- [12] P.P. Wulan, T.P.J. Silaen, Synthesis of ACNT on quartz substrate with catalytic decomposition reaction from *Cinnamomum camphora* by using FC-CVD method, *AIP Conf. Proc.* 1840, (2017) 080003-1-080003-8.
- [13] Y. Li, G. Xu, H. Zhang, T. Li, Y. Yao, Q. Li, Z. Dai, Alcohol-assisted rapid growth of vertically aligned carbon nanotube arrays, *Carbon*, 91 (2015) 45-55.
- [14] Q. Wen, R. Zhang, W. Qian, Y. Wang, P. Tan, J. Nie, F. Wei, Growing 20 cm long DWNTs/TWNTs at a rapid growth rate of 80-90  $\mu\text{m/s}$ , *Chem. Mater.* 22 (2010) 1294-1296.
- [15] G.-Y. Xiong, D. Wang, Z. Ren, Aligned millimeter-long carbon nanotube arrays grown on single crystal magnesia, *Carbon*, 44 (2006) 969-973.
- [16] W. Zhou, Z. Han, J. Wang, Y. Zhang, Z. Jin, X. Sun, Y. Zhang, C. Yan, Y. Li, Copper catalyzing growth of single-walled carbon nanotubes on substrates, *Nano Lett.* 6 (2006) 2987-2990.
- [17] Q. Li, X.F. Zhang, R.F. DePaula, L.X. Zheng, Y.H. Zhao, L. Stan *et al.*, Sustained growth of ultralong carbon nanotube arrays for fiber spinning, *Adv. Mater.* 18 (2006) 3160-3163.
- [18] E. Einarsson, Y. Murakami, M. Kadowaki, S. Maruyama, Growth dynamics of vertically aligned single-walled carbon nanotubes from in situ measurements, *Carbon*, 46 (2008) 923-930.
- [19] E.R. Meshot, D.L. Plata, S. Tawfick, Y. Zhang, E.A. Verploegen, A.J. Hart, Engineering vertically aligned carbon nanotube growth by decoupled thermal treatment of precursor and catalyst, *ACS Nano*, 3 (2009) 2477-2486.
- [20] B.H. Choi, H. Yoo, Y.B. Kim, J.H. Lee, Effects of Al buffer layer on growth of highly vertically aligned carbon nanotube forests for in situ yarning, *Microelectron. Eng.* 87 (2010) 1500-1505.
- [21] G.D. Nessim, A. Al-Obeidi, H. Grisaru, E.S. Polsen, C.R. Oliver, T. Zimrin *et al.*, Synthesis of tall carpets of vertically aligned carbon nanotubes by in situ generation of water vapor through preheating of added oxygen, *Carbon*, 50 (2012) 4002-4009.
- [22] M.Z. Naghadehi, M. Samaei, M. Ranjbarnia, V. Nourani, State-of-the-art predictive modeling of TBM performance in changing geological conditions through gene expression programming. 126 (2018) 46-57.
- [23] A.H. Gandomi, A.H. Alavi, S. Kazemi, M. Gandomi, Formulation of shear strength of slender RC beams using gene expression programming, part I: Without shear reinforcement, *Automat. Constr.* 42 (2014) 112-121.
- [24] E. Momeni, R. Nazir, D.J. Armaghani, H. Maizir, Prediction of pile bearing capacity using a hybrid genetic algorithm-based ANN, *Measurement*, 57 (2014) 122-131.
- [25] A. Shafaei, G.R. Khayati, A predictive model on size of silver nanoparticles prepared by green synthesis method using hybrid artificial neural network-particle swarm optimization algorithm, *Measurement*, 150 (2020) 107199.
- [26] M.M. Jafari, G.R. Khayati, M. Hosseini, H. Danesh-Manesh, Modeling and optimization of roll-bonding parameters for bond strength of Ti/Cu/Ti clad composites by artificial neural networks and genetic algorithm, *Int. J. Eng. Trans. C*, 30 (2017) 1885-1893.
- [27] K. Patra, A.K. Jha, T. Szalay, J. Ranjan, L. Monostori, Artificial neural network based tool condition monitoring in micro mechanical peck drilling using thrust force signals, *Precis. Eng.* 48 (2017) 279-291.
- [28] V. Rajamohan, R. Sedaghati, S. Rakheja, Optimum design of a multilayer beam partially treated with magnetorheological fluid, *Smart Mater. Struct.* 19 (2010) 065002.
- [29] M. Zeraati, G.R. Khayati, N. Materials, Optimization of micro hardness of nanostructure Cu-Cr-Zr alloys prepared by the mechanical alloying using artificial neural networks and genetic algorithm, *Journal of Ultrafine Grained and Nanostructured Materials*, 51 (2018) 183-192.
- [30] P. Zhu, S. Zhou, J. Zhen, Y. Li, Application of artificial neural network in composite research. In: Tan Y., Shi Y., Tan K.C. (eds), *Advances in Swarm Intelligence, ICSI 2010, Lecture Notes in Computer Science*, 6146 (2010) 558-563.
- [31] J. Kennedy, R. Eberhart, Particle swarm Optimization, in *Proceedings of IEEE International Conference on Neural Networks IV*, 1995.
- [32] R.R. Karri, J. Sahu, Modeling and optimization by particle swarm embedded neural network for adsorption of zinc (II) by palm kernel shell based

- activated carbon from aqueous environment, Journal of environmental management. 206 (2018) 178-191.
- [33] S. Du, W. Li, K. Cao, A learning algorithm of artificial neural network based on GA-PSO, 2006 6<sup>th</sup> World Congress on Intelligent Control and Automation, Dalian, 2006, pp. 3633-3637.
- [34] X.H. Shi, Y.H. Lu, C.G. Zhou, H.P. Lee, W.Z. Lin Y.C. Liang, Hybrid evolutionary algorithms based on PSO and GA, The 2003 Congress on Evolutionary Computation (CEC '03), Canberra, ACT, Australia, Vol.4 (2003) pp. 2393-2399.
- [35] G.-G. Wang, A.H. Gandomi, X.-S. Yang, A.H. Alavi, A novel improved accelerated particle swarm optimization algorithm for global numerical optimization, Eng. Computation. 31 (2014) 1198-1220.
- [36] J.R. Koza, Genetic Programming II, Automatic Discovery of Reusable Subprograms, MIT Press, Cambridge, MA, 1194.
- [37] İ. Karahan, R. Özdemir, A new modeling of electrical resistivity properties of ZnFe alloys using genetic programming, Optoelectron. Adv. Mat. 4 (2010) 812-815.
- [38] A.H. Gandomi, D.A. Roke, Assessment of artificial neural network and genetic programming as predictive tools, Adv. Eng. Softw. 88 (2015) 63-72.
- [39] S.N. Sivanandam, S.N. Deepa, Genetic algorithm optimization problems, in Introduction to Genetic Algorithms, Springer, 2008, pp. 165-209.
- [40] M.İ. Coşkun, İ.H. Karahan, Modeling corrosion performance of the hydroxyapatite coated CoCrMo biomaterial alloys, J. Alloy. Compd. 745 (2018) 840-848.
- [41] Y. Benjamini, Opening the box of a boxplot, Am. Stat. 42 (1988) 257-262.
- [42] B. Tiryaki, Predicting intact rock strength for mechanical excavation using multivariate statistics, artificial neural networks, and regression trees, Eng. Geol. 99 (2008) 51-60.
- [43] A.R. Sayadi, M.R. Khalesi, M.K. Borji, A parametric cost model for mineral grinding mills, Miner. Eng. 55 (2014) 96-102.
- [44] A.R. Sayadi, A. Lashgari, J.J. Paraszczak, Hard-rock LHD cost estimation using single and multiple regressions based on principal component analysis, Tunn. Undergr. sp. Tech. 27 (2012) 133-141.
- [45] H.F. Kaiser, An index of factorial simplicity, Psychometrika, 39 (1974) 31-36.
- [46] R.S. Faradonbeh, M. Monjezi, Prediction and minimization of blast-induced ground vibration using two robust meta-heuristic algorithms, Eng. Comput. 33 (2017) 835-851.
- [47] O. Nerushev, S. Dittmar, R.-E. Morjan, F. Rohmund, E.E.B. Campbell, Particle size dependence and model for iron-catalyzed growth of carbon nanotubes by thermal chemical vapor deposition, J. Appl. Phys. 93 (2003) 4185-4190.
- [48] R. Morjan, O.A. Nerushev, M. Sveningsson, F. Rohmund, L.K.L. Falk, E.E.B. Campbell, Growth of carbon nanotubes from C<sub>60</sub>, Appl. Phys. 78 (2004) 253-261.
- [49] M. Kumar, Y. Ando, Chemical vapor deposition of carbon nanotubes: a review on growth mechanism and mass production, J. Nanosci. Nanotechnol. 10 (2010) 3739-3758.
- [50] F. Ding, P. Larsson, J.A. Larsson, R. Ahuja, H. Duan, A. Rosén, K. Bolton, The importance of strong carbon-metal adhesion for catalytic nucleation of single-walled carbon nanotubes, Nano Lett. 8 (2008) 463-468.